



Cite this: DOI: 10.1039/d5nj04118j

Synthesis and characterization of 5,15-bis(hydroxymethyl)porphyrins – simple compounds distantly inspired by the chlorosomal bacteriochlorophylls

Vy-Phuong Tran, ^a Arup Kundu, ^b Madelyn N. Scott, ^b Ainsley Iwanicki, ^b Phattananawee Nalaoh, ^c James R. Diers, ^d Masahiko Taniguchi, ^a David F. Bocian, ^d Gabriela S. Schlau-Cohen ^{*b} and Jonathan S. Lindsey ^{*a}

A self-assembly paradigm is provided in green photosynthetic bacteria by the chlorin macrocycle bacteriochlorophyll (BChl) *c*, which contains a 3-(1-hydroxyethyl) substituent, central magnesium ion, and 13-keto group. The assembled BChl *c* structure is a powerful light-harvesting apparatus that can support life even under extreme low-light conditions. Here, inspired by the work of Balaban, two far simpler porphyrins have been synthesized, 5,15-bis(hydroxymethyl)-10,20-diphenylporphinatozinc(II) (**Ph/CH₂OH**) and 5,15-bis(hydroxymethyl)porphinatozinc(II) (**H/CH₂OH**), and analogues wherein ethyl replaces hydroxymethyl (**Ph/Et** and **H/Et**). Examination of **Ph/CH₂OH** and **H/CH₂OH** by time-resolved spectroscopy showed an ~2-fold enhancement in the singlet excited-state lifetime compared to *meso*-tetraphenylporphinatozinc(II) (**ZnTPP**). The single-crystal X-ray diffraction revealed distinct packing patterns. Porphyrin **Ph/CH₂OH** exhibited double staircases wherein (1) each zinc is pentacoordinate (by apical coordination of one hydroxymethyl group of a porphyrin in the same staircase), (2) the second hydroxymethyl group is hydrogen-bonded to an apically coordinated hydroxymethyl oxygen atom in the adjacent staircase, (3) the porphyrins in a given staircase are coplanar but cofacially offset with each other, and (4) the adjacent staircases are oriented approximately 72° relative to each other. Porphyrin **H/CH₂OH** assembled wherein (1) each zinc is hexacoordinate by ligation of hydroxymethyl moieties, (2) each hydroxymethyl –OH is hydrogen-bonded with an acetonitrile solvent molecule in the lattice, and (3) the planes of the four nearest neighbor porphyrins are essentially perpendicular to a given porphyrin. Study of the solid-state packing patterns of sparsely substituted porphyrins enables insights into how the structural design of tetrapyrroles can guide their aggregate self-assembly.

Received 18th October 2025,
Accepted 27th December 2025

DOI: 10.1039/d5nj04118j

rsc.li/njc

Introduction

Chlorophylls and bacteriochlorophylls are the key components of photosynthetic antenna complexes that absorb light and funnel excitation energy to the reaction centers.¹ A general strategy found in plants and purple bacteria relies on (bacterio)-chlorophylls embedded in pigment-binding proteins in elaborate 3-dimensional structures. In green photosynthetic bacteria, by contrast, the tetrapyrrole pigments self-associate to give green

bodies (*i.e.*, chlorosomes) with little proteinaceous scaffolding.² The resulting highly organized molecular architecture supports efficient energy transfer and thereby provides the basis for a light-harvesting antenna. A representative self-assembling macrocycle is bacteriochlorophyll *c*, a dihydroporphyrin that is equipped with a 3-(1-hydroxyethyl) group, a 13-keto group as part of the isocyclic ring, and the centrally chelated magnesium(II) ion (Fig. 1).³ The proposed organization entails a layered stack of relatively coplanar and cofacially offset macrocycles. The proposed intermolecular interactions that engender the organization include the combination of (i) apical coordination of the magnesium(II) ion by the 3-(1-hydroxyethyl) group of a neighboring macrocycle, (ii) hydrogen-bonding of the hydroxyl group with the keto group of yet another macrocycle, and (iii) π – π stacking.⁴

Much effort has been devoted to understand the essential structural features that undergird the assembly into functional light-harvesting antennas. Tamiaki has employed semisynthesis

^a Department of Chemistry, North Carolina State University, Raleigh, NC 27695, USA. E-mail: jlindsey@ncsu.edu

^b Department of Chemistry, Massachusetts Institute of Technology, Cambridge, Massachusetts 02139, USA. E-mail: gssc@mit.edu

^c Department of Chemistry, University of Tennessee, Knoxville, TN 37996, USA. E-mail: pnalaoh@utk.edu

^d Department of Chemistry, University of California, Riverside, California 92521-0403, USA. E-mail: david.bocian@ucr.edu



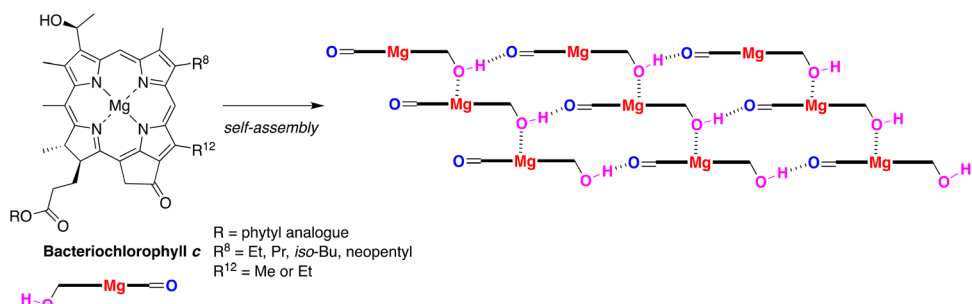


Fig. 1 Native bacteriochlorophyll c and proposed molecular interactions in the self-assembly.⁴ Many substituents are omitted for clarity.

with derivatives of natural pigments to create diverse macrocycles for probing the role of structural substituents on the self-assembly pattern.^{5–12} Balaban pioneered the design and synthesis of a set of far simpler porphyrins, which upon self-assembly give broad and red-shifted absorption maxima.^{9,13–21} The evolution of the Balaban design is shown in the 10,20-diaryl family by the 3,13-substitution pattern of **I**,¹⁴ the 3,15-substitution pattern of **II**,¹⁵ and **III**,⁴ and the 5,15-substitution pattern of **IV**,¹⁴ **V**,¹⁴ and **VI**²² (Chart 1). The 3,13-substitution pattern also was examined in the β -substituted porphyrin **VII**.¹⁴ In all cases, the zinc chelate was employed as a chemically more

robust surrogate for magnesium. Among this set, porphyrins **III**,⁴ **IV**,¹⁶ and **VI**⁴ have been characterized by single-crystal X-ray diffraction (SCXRD) analysis. The pioneering work of Balaban (1958–2016) was left undeveloped owing to his untimely passing.²³

The question of interest here is whether even simpler molecular designs can afford chlorosomal-like assemblies. In this work, four *meso*-substituted zinc(II)porphyrins have been synthesized (Chart 1). Two porphyrins contain 5,15-dihydroxymethyl groups with the presence of 10,20-diphenyl groups (**Ph/CH₂OH**) or with the lack of 10,20-diphenyl group (**H/CH₂OH**). Two other

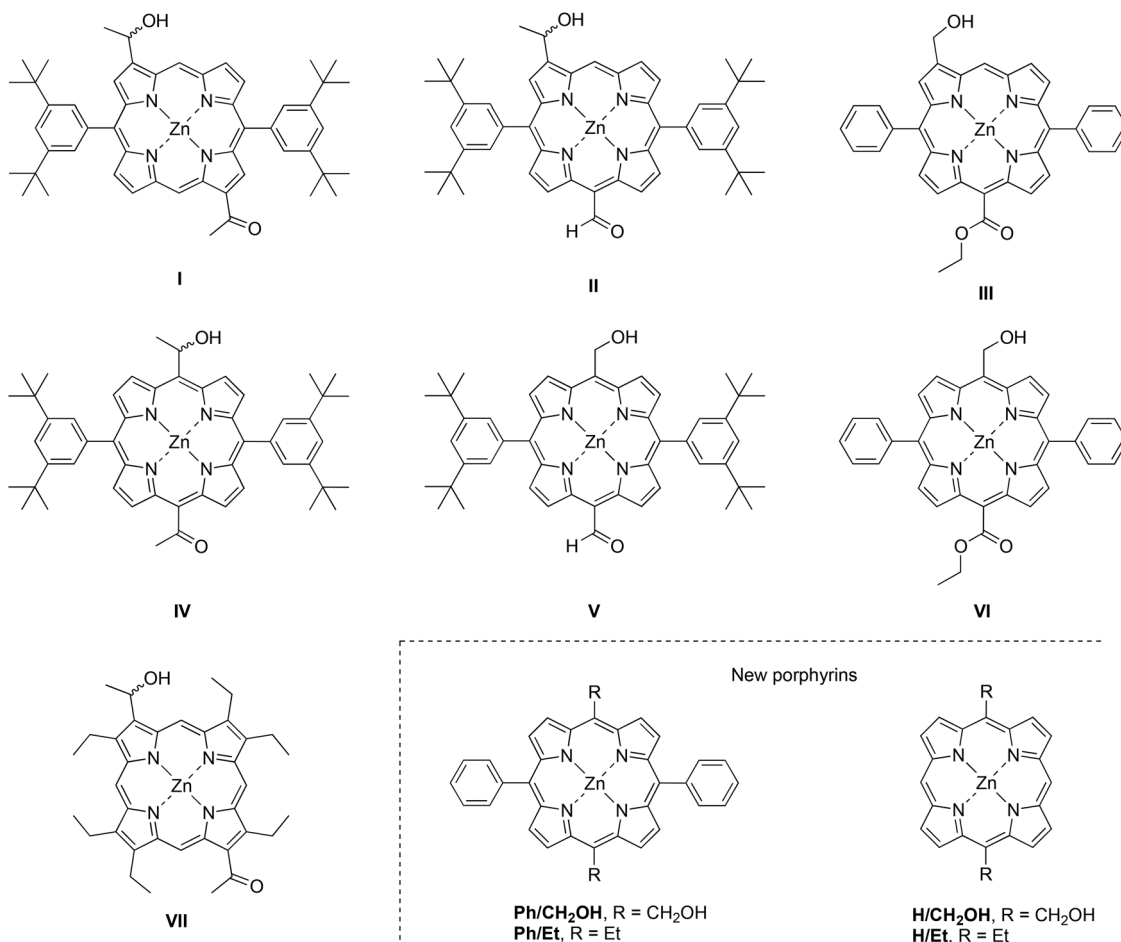


Chart 1 Porphyrins bearing hydroxylalkyl substituents for possible self-assembly.



porphyrins (**Ph/Et**, **H/Et**) have identical substitution patterns but with an ethyl group in place of the hydroxymethyl substituent. The electronic properties and dynamics of the synthetic porphyrins have been characterized by steady-state and time-resolved spectroscopy. All four porphyrins were also analyzed by SCXRD for comparative assessment of their structural packing patterns. The results provide insights into the relationship between the structure and assembly of simple compounds as putative analogs of chlorosomal bacteriochlorophylls.

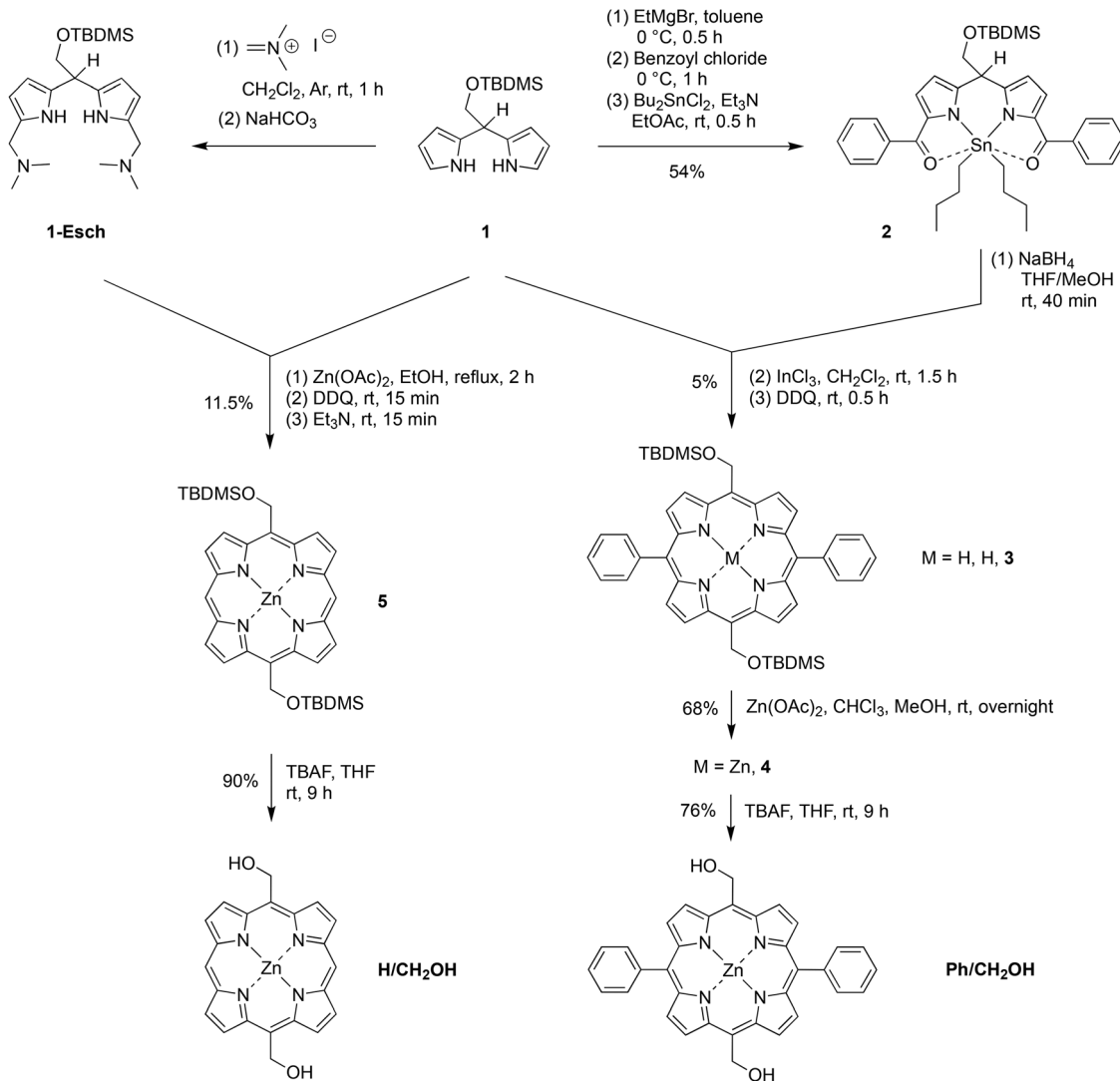
Results

Synthesis

Porphyrin **Ph/CH₂OH** is a *trans*-A₂B₂-porphyrin whereas porphyrin **H/CH₂OH** is a *trans*-A₂-porphyrin, where A is a hydroxymethyl group and B is a phenyl group (Scheme 1). Dipyrromethane building blocks that bear various one-carbon units are key to the general synthetic approach. The *tert*-butyldimethylsilyl (TBDMS)-protected 5-hydroxymethyldipyrromethane **1** comprises a key

building block and has been prepared and used previously in the synthesis of **I**. The unprotected 5-hydroxymethyldipyrromethane also has been employed.²⁴ Dipyrromethane **1** has been converted in 54% yield to the 1,9-dibenzoyl derivative complexed with dibutyltin (**2**), where the tin complexation affords a crystalline product that is readily purified.²² Treatment of **2** with NaBH₄ afforded the corresponding dipyrromethane-1,9-dicarbinol (and concomitant loss of dibutyltin), which upon condensation with dipyrromethane **1** in the presence of InCl₃ followed by oxidation with 2,3-dichloro-5,6-dicyano-1,4-benzoquinone (DDQ) afforded free base porphyrin **3** (5%). Subsequent reaction with Zn(OAc)₂ gave zinc porphyrin **4** (68%). The TBDMS group was removed upon treatment with tetrabutylammonium fluoride (TBAF) to afford the target porphyrin **Ph/CH₂OH** (76%). It should be mentioned that an attempt to condense **1** and benzaldehyde in the presence of BF₃·OEt₂ was not effective, which prompted pursuit of the route reported here.

For the synthesis of porphyrin **H/CH₂OH**, dipyrromethane **1** was treated with Eschenmoser's reagent to give the



Scheme 1 Synthesis of bis(hydroxymethyl)porphyrins.



1,9-bis(dimethylaminomethyl)-substituted dipyrromethane as the bis(hydroiodide) salt. Treatment of the reaction mixture with saturated aqueous NaHCO_3 liberated the free base dipyrromethane **1-Esch** from the bis(hydroiodide) salt. Dipyrromethane **1-Esch** was not characterized but was reacted *in situ* with dipyrromethane **1** in the standard way²⁵ to form zinc porphyrin **5** in 11.5% yield. Deprotection with TBAF gave zinc porphyrin **H/CH₂OH** in 90% yield.

An established route to dipyrromethane-1-carbinols was applied for the synthesis of porphyrin **Ph/Et**. The *meso*-ethyl-dipyrromethane²⁶ **6** was treated with EtMgBr followed by pyridyl thioester²⁷ **7** to obtain 1-acyldipyrromethane **8** in 90% yield (Scheme 2). Reduction of **8** gave the dipyrromethane-1-carbinol, which was condensed in the presence of InCl_3 to afford the *trans*- A_2B_2 -porphyrin, 5,15-diethyl-10,20-diphenylporphyrin (**9**), in 37% yield. Subsequent reaction with $\text{Zn}(\text{OAc})_2$ gave the target zinc(II) chelate **Ph/Et** in (80%).

The *meso*-ethyldipyrromethane²⁶ **6** also was treated with the Eschenmoser reagent to give the 1,9-bis(*N,N*-dimethylamino-methyl)dipyrromethane **6-Esch**. Treatment to the standard conditions established in the Eschenmoser route with dipyrromethane **6** gave zinc porphyrin **H/Et** in 8.3% yield.

Each porphyrin was characterized by ¹H NMR spectroscopy, ¹³C{¹H} NMR spectroscopy, high-resolution mass spectrometry *via* electrospray ionization-time-of-flight (HRMS *via* ESI-TOF), matrix-assisted laser desorption ionization mass spectrometry (MALDI-MS),²⁸ and absorption and fluorescence spectroscopy. The symmetry and sparse substitution of each of the four porphyrins afford simple and readily interpretable ¹H NMR spectra (Fig. S1). The results from absorption and fluorescence spectroscopy are described in the next section.

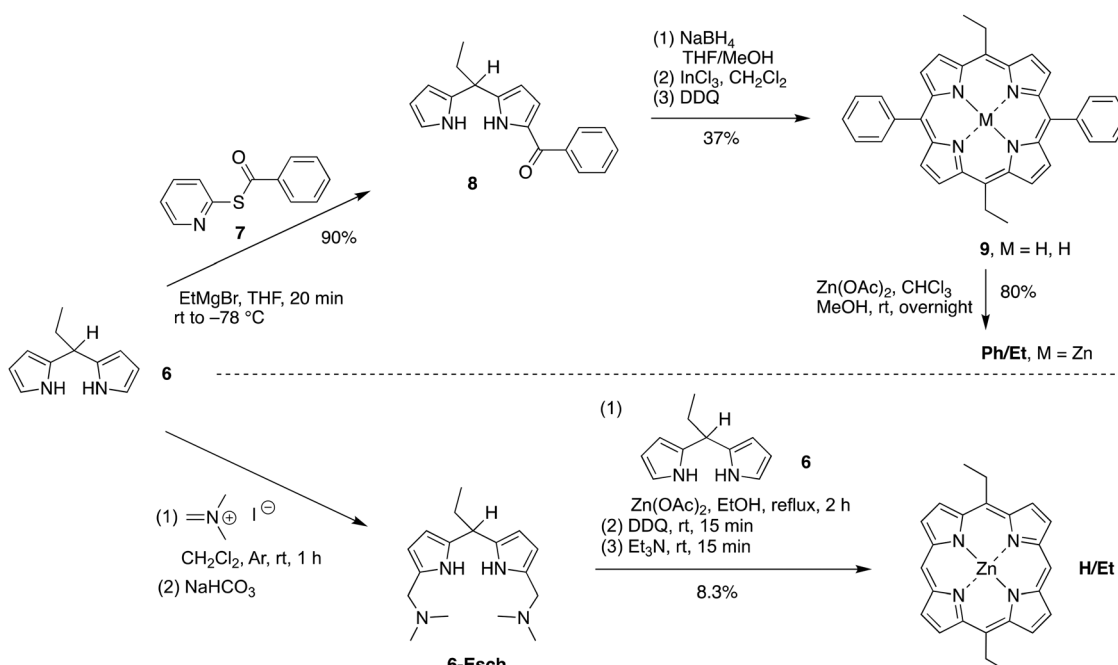
Spectroscopic characterization

Steady-state features. The steady-state absorption spectra of the four zinc porphyrins (**Ph/CH₂OH**, **Ph/Et**, **H/CH₂OH**, **H/Et**) were collected in tetrahydrofuran (THF) solution under ambient conditions without deaeration (“aerated”). In contrast with the homogeneous solutions in THF, attempts to use toluene or dichloromethane for all four zinc porphyrins resulted in incomplete solubilization (*e.g.*, cloudy suspensions) and/or highly broadened spectra indicative of aggregation; on the other hand, addition thereto of a small amount of THF typically afforded homogeneous solutions. For the free base porphyrins, homogeneous solutions were obtained in toluene without THF.

All of the following data for the four zinc porphyrins were obtained in aerated neat THF solution. Each porphyrin exhibits the characteristic B-band (Soret or $S_0 \rightarrow S_2$) and Q-band ($S_0 \rightarrow S_1$) transitions. The Q-band transitions exhibit a vibronic progression, denoted as Q(0,0) and Q(1,0) for the transitions with zero and one vibrational quanta (respectively), with a spacing ranging from ~ 950 – 1280 cm^{-1} for each porphyrin (Fig. 2). Expanded spectra are provided in Fig. S2–S6. The spectral features are summarized in Table 1. Several trends are evident.

• First, the porphyrins with four *meso*-substituents (**Ph/CH₂OH**, **Ph/Et**) exhibit B (421, 424 *versus* 408, 410 nm) and Q(1,0) (555, 558 *versus* 543, 546 nm) bands at longer wavelength than porphyrins with two *meso*-substituents (**H/CH₂OH**, **H/Et**). Such shifts are consistent with the previous observation of a systematic bathochromic shift in the absorption spectra of zinc porphyrins with an increase in the number of substituted phenyl groups.²⁹

• Second, the addition of an ethyl group instead of a hydroxymethyl group generally causes a bathochromic shift of several nanometers for the B and Q bands, although one apparent



Scheme 2 Synthesis of 5,15-diethylporphyrins.



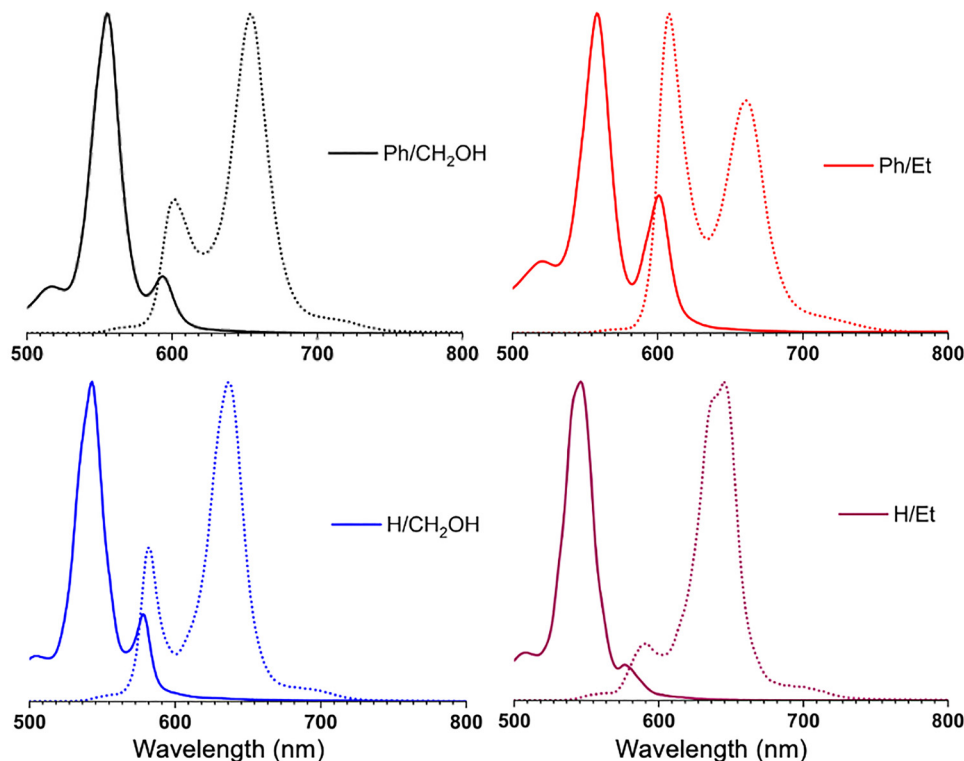


Fig. 2 Absorption spectra (solid lines) of the Q-band region and fluorescence spectra (dashed lines) of the four synthetic porphyrins in aerated THF solution at room temperature.

Table 1 Absorption and fluorescence properties^a

Sample	λ_{abs} , nm			λ_{em} , nm			Stokes shift, cm^{-1}	$I_{\text{Q}(1,0)}/I_{\text{Q}(0,0)}$ ^b
	B	Q(1,0)	Q(0,0)	Q(0,0)	Q(0,1)	$I_{\text{B}(0,0)}/I_{\text{Q}(1,0)}$ ^b		
Ph/CH ₂ OH	421	555	594	602	654	23	224	5.7
Ph/Et	424	558	601	607	661	28	164	2.4
H/CH ₂ OH	408	543	578	582	637	29	119	3.7
H/Et	410	546	576	591	645	30	441	9.0
ZnTPP	423	555	595	603	655	31	223	3.2

^a All data were obtained in aerated THF solution at room temperature.

^b Ratio of peak intensities.

Table 2 Singlet excited-state properties^a

Sample	τ (ns)	Φ_f	τ° (ns)	k_r (s^{-1})	k_{nr} (s^{-1})
Ph/CH ₂ OH	3.7	0.039	100	1.0×10^7	26×10^7
Ph/Et	2.03	0.026	78	1.3×10^7	48×10^7
H/CH ₂ OH	4.2	0.042	102	0.98×10^7	23×10^7
H/Et	3.0	0.024	130	0.77×10^7	33×10^7
ZnTPP	1.87	0.026	72	1.4×10^7	52×10^7

^a All data were obtained in aerated THF solution at room temperature. Lifetimes were obtained from time-correlated single-photon counting (TCSPC) measurements. Fluorescence lifetime, τ ; fluorescence quantum yield, Φ_f ; radiative lifetime, τ° ; radiative decay rate, k_r ; nonradiative decay rate, k_{nr} .

exception is the Q(0,0) band of **H/Et** (576 nm) *versus* **H/CH₂OH** (578 nm); this may simply reflect the relatively very weak band Q(0,0) band on the tail of the more intense Q(1,0) band of **H/Et**.

• Third, the relative intensity of the Q(0,0) band is sensitive to the nature of the substituents, as is seen by the ratio of the intensities of the Q(1,0) and Q(0,0) bands, which ranges from 2.4 for **Ph/Et** to 9.0 for **H/Et**.

Excited-state features. The fluorescence quantum yield (Φ_f) values were measured of porphyrins **Ph/CH₂OH** and **H/CH₂OH**, along with their analogues **Ph/Et** and **H/Et**, using **ZnTPP** in aerated THF as a reference (Table 2 and Table S1). Porphyrins **Ph/CH₂OH** and **H/CH₂OH** demonstrated enhanced fluorescence quantum yields (0.039 and 0.042, respectively) relative to **ZnTPP** (0.026).³⁰ In contrast, **Ph/Et** and **H/Et** exhibited comparable or decreased quantum yields (0.026 and 0.024, respectively) relative to **ZnTPP**. Such changes in the fluorescence quantum yield can be attributed to changes in the radiative and nonradiative dissipation pathways (*vide infra*).

Time-resolved fluorescence measurements were performed in aerated THF. The decay curves were well-fit with a monoexponential function (Fig. S7). The extracted decay timescales were 3.7 ns and 4.2 ns for the hydroxymethylporphyrins **Ph/CH₂OH** and **H/CH₂OH**, respectively. For analogues **Ph/Et** and **H/Et**, where the hydroxymethyl groups were replaced by ethyl groups, the timescales were slightly shorter, 2.03 and 3.0 ns, respectively. The reference compound **ZnTPP** exhibited a lifetime value of 1.87 ns, which closely resembles the reported consensus value of 2.0 ns (in aerated toluene).³⁰

To understand the origin of the enhanced fluorescence observed in **Ph/CH₂OH** and **H/CH₂OH**, the measured emission lifetime and fluorescence quantum yield of each compound

were used to calculate the radiative and nonradiative decay rates of the singlet excited state (eqn (S1)–(S3); Table 2). The nonradiative decay rates for **Ph/CH₂OH** and **H/CH₂OH** (26×10^7 s⁻¹ and 23×10^7 s⁻¹, respectively) were diminished with respect to **ZnTPP** (52×10^7 s⁻¹). Further, the radiative decay rates also decreased for **Ph/CH₂OH** and **H/CH₂OH** (1.0×10^7 s⁻¹ and 0.98×10^7 s⁻¹, respectively) relative to **ZnTPP** (1.4×10^7 s⁻¹). The porphyrin analogues **Ph/Et** and **H/Et** follow a similar trend, albeit to a lesser degree than **Ph/CH₂OH** and **H/CH₂OH**. These distinctions are attributed to differences in the nonradiative rates, which has two components, internal conversion (IC) and intersystem crossing (ISC). The rate of IC often approximately scales with the number of normal modes,

but no correlation was observed between the nonradiative rate and the number of normal modes, and indeed, the overall Q(1,0) vibronic structure was similar for all four porphyrins. The yield of ISC, which is quite high in zinc porphyrins (88% for **ZnTPP**)²⁹ is likely the dominant factor, although the rationale for this is not clear.

To resolve the initial excited-state dynamics, porphyrins **Ph/CH₂OH** and **H/CH₂OH** in aerated THF were examined by femtosecond transient absorption (fs-TA) measurements. The excited-state dynamics of the porphyrin solutions were probed using a broadband white light supercontinuum (~ 400 nm to 800 nm) subsequent to 400 nm excitation, resonant with the B band. Fig. 3a shows the fs-TA spectra traces for **Ph/CH₂OH** and

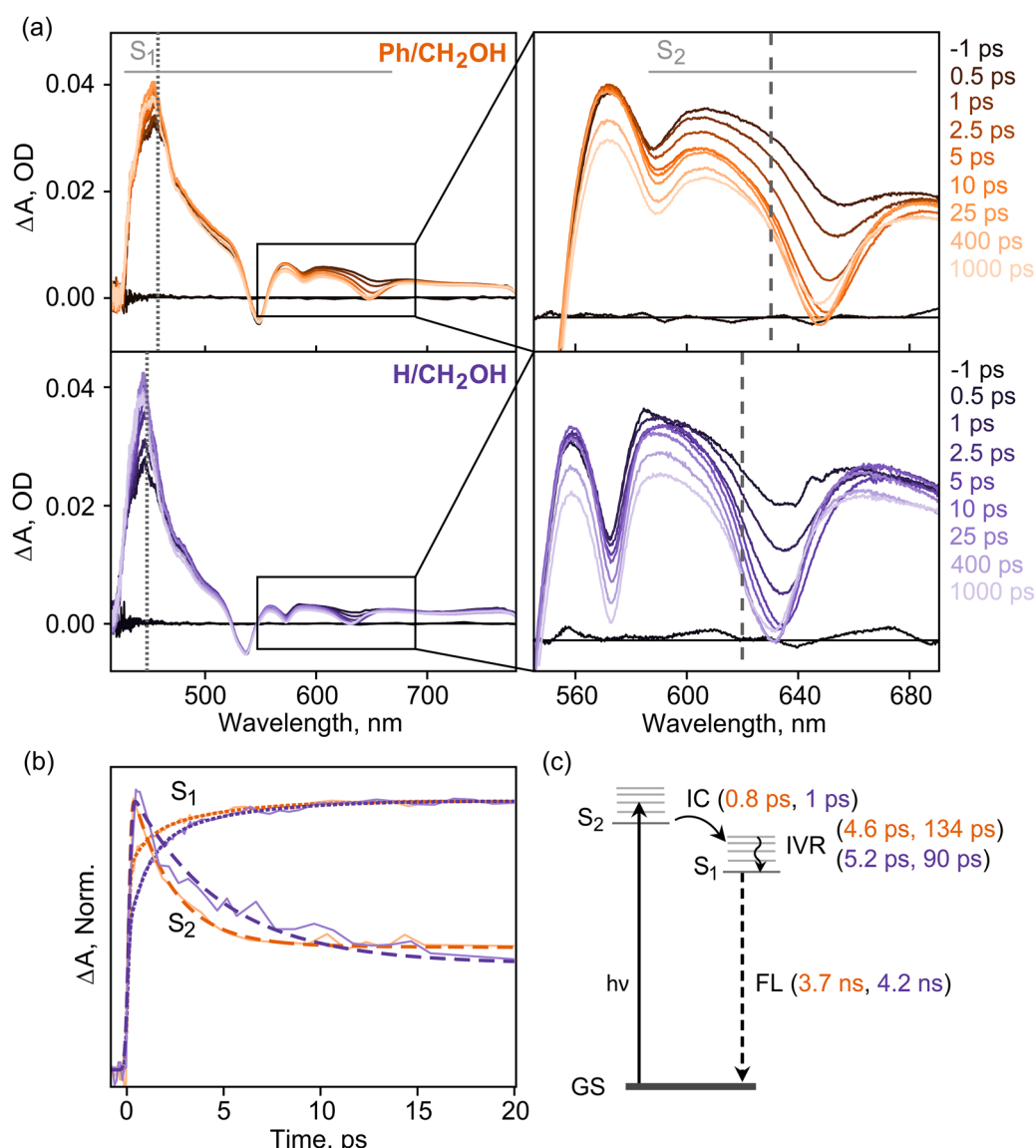


Fig. 3 Femtosecond transient absorption spectroscopy of the porphyrins. (a) Broadband transient absorption spectra ($\lambda_{\text{pump}} = 400$ nm) of **Ph/CH₂OH** and **H/CH₂OH** in aerated THF solution (20 μM). Zoom in on the ΔA spectra of the Q band. (b) Comparative single-point decay kinetics of **Ph/CH₂OH** and **H/CH₂OH** showing the $S_2 \rightarrow S_1$ transition. The kinetic traces are collected at 457 nm and 630 nm for **Ph/CH₂OH** and 447 nm and 620 nm for **H/CH₂OH**, respectively, shown by dotted vertical lines in (a). (c) Kinetic model for excited-state dynamics of **Ph/CH₂OH** and **H/CH₂OH** in solution. IC, internal conversion; IVR, intramolecular vibrational relaxation; FL, fluorescence.



H/CH₂OH at representative time delays from -1 ps to 1000 ps. The timescales of the dynamics were extracted with multi-exponential kinetic fitting (Fig. 3b).

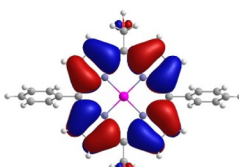
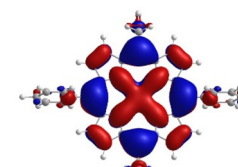
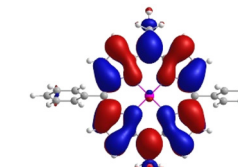
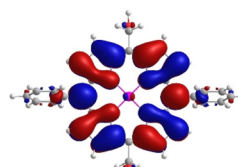
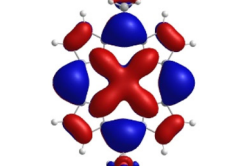
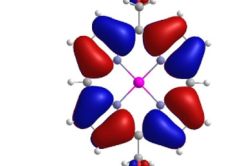
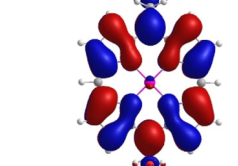
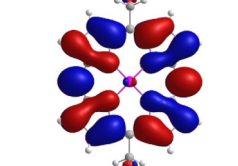
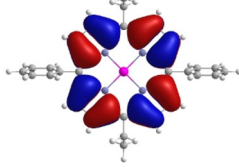
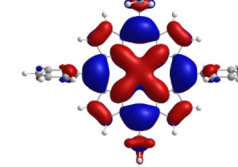
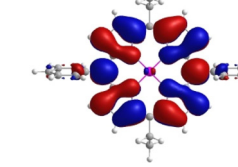
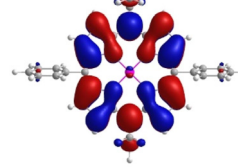
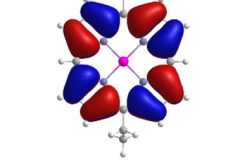
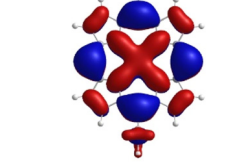
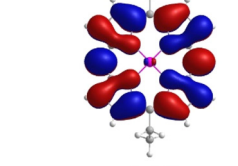
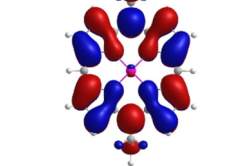
After initial photoexcitation, a broad excited-state absorption (ESA) feature was present in the spectral region of 415 nm to 780 nm for both the porphyrins, along with a strong ground-state bleach (GSB) of the Q bands at 548 nm for **Ph/CH₂OH** and 536 nm for **H/CH₂OH**, respectively. The initial broad ESA feature is assigned to a photoexcited S_2 state, which evolves to the S_1 state *via* IC. The IC of the $S_2 \rightarrow S_1$ was observed as a rise in a sharp ESA feature associated with the S_1 state around 450 nm and a concomitant decay of the stimulated emission (SE) feature of the S_2 state around 545 nm to 690 nm (Fig. 3a, left panel). Time constants of 0.8 ps and 1 ps were extracted for $S_2 \rightarrow S_1$ IC in **Ph/CH₂OH** and **H/CH₂OH**, respectively. The subsequent two time constants were assigned to intramolecular vibrational relaxation (IVR) in the S_1 state (4.6 ps and 134 ps for **Ph/CH₂OH**, 5.2 ps and 90 ps for **H/CH₂OH**). The slowest time constant (> 2 ns) was assigned to the formation of a long-lived triplet state *via* ISC. These dynamics are summarized in Fig. 3c and are consistent with earlier reports on zinc porphyrins.^{31,32}

Timescales obtained through the fs-TA measurements were consistent with those obtained *via* time-resolved fluorescence, revealing that these zinc porphyrins show an enhancement of up to 2-fold in the singlet excited-state lifetime as compared to traditional **ZnTPP** systems. The long-lived excited-state has the potential to enhance energy transport for synthetic light-harvesting systems and other optoelectronic applications.

Molecular orbital characteristics and absorption spectra simulations

Density functional theory (DFT) calculations³³ were performed on the zinc porphyrins **Ph/CH₂OH**, **Ph/Et**, **H/CH₂OH**, and **H/Et**. The energies and electron density distributions of the four frontier molecular orbitals (MOs) are shown in Table 3. The characteristics of the MOs are typical of porphyrins wherein the macrocycles exhibit approximate two-fold or higher symmetry.³⁴ In particular, the highest occupied molecular orbitals (HOMOs) are a_{1u} - and a_{2u} -like, and the lowest unoccupied molecular orbitals (LUMOs) are e_g -like (D_{4h} notation). For **Ph/CH₂OH**, **Ph/Et**, and **H/Et**, the HOMO is a_{2u} -like and the HOMO-1 is a_{1u} -like. This pattern is reversed for **H/CH₂OH**. For **Ph/CH₂OH** and

Table 3 Energies and electron density distributions for the frontier MOs of four zinc porphyrins

Porphyrins	HOMO-1/eV	HOMO/eV	LUMO/eV	LUMO+1/eV
Ph/CH₂OH	 -6.87	 -6.85	 -1.23	 -1.09
	 -6.95	 -6.87	 -1.22	 -1.06
Ph/Et	 -6.87	 -6.65	 -1.09	 -1.07
	 -6.87	 -6.74	 -1.05	 -1.05



H/CH₂OH, the vertical symmetry plane of the e_g -like LUMO passes through the 5,15-*meso*-carbon atoms and the plane of the e_g -like LUMO+1 passes through the 10,20-*meso*-carbon atoms. This pattern is reversed for **Ph/Et** and **H/Et**.

The absorption spectra of the four porphyrins were simulated using the Gouterman module in PhotochemCAD.³⁵ This calculation utilizes the four frontier MOs shown in Table 3. The calculations faithfully reproduce the relative energies of the B(0,0) and Q(0,0) bands of the four porphyrins (Fig. S8–S10). In particular, the calculations reproduce the observed bathochromic shift of the 10,20-phenyl-substituted molecules (**Ph/CH₂OH** and **Ph/Et**) relative to those that lack these substituents (**H/CH₂OH** and **H/Et**), as well as the additional bathochromic shifts observed upon ethyl replacement of the hydroxymethyl groups: larger in **Ph/Et** versus **Ph/CH₂OH** than in **H/Et** versus **H/CH₂OH**. More interestingly, the calculation reproduces the observed relative intensities of the Q(0,0) bands of the four porphyrins **Ph/Et** > **H/CH₂OH** > **Ph/CH₂OH** > **H/Et** (Table 1). This pattern reflects the observation that ethyl replacement of the hydroxymethyl groups in the 10,20-phenyl-substituted porphyrins (**Ph/Et** versus **Ph/CH₂OH**) increases the intensity of the Q(0,0) absorption, whereas this substitution in the porphyrins that lack the phenyl groups (**H/Et** versus **H/CH₂OH**) decreases the intensity of the Q(0,0) band. The rank ordering of the porphyrins on the basis of the relative intensity of the Q(0,0) absorption transition (**Ph/Et** > **H/CH₂OH** > **Ph/CH₂OH** > **H/Et**) nearly parallels that of the magnitude of the radiative rate constant (k_f , Table 2) (**Ph/Et** > **Ph/CH₂OH** ~ **H/CH₂OH** > **H/Et**).

Single-crystal X-ray analysis

Each porphyrin was crystallized from THF upon slow vapor diffusion with an antisolvent (hexane, heptane, acetone, or acetonitrile) and analyzed by SCXRD. The full crystal structure data for the four

porphyrins are provided in Tables S2–S5. The salient results for each porphyrin are provided here. In the following text, the mean plane is described by the carbon skeleton (C1, C2, C3, C4, ..., C19, C20) of the porphyrin macrocycle.

Porphyrin **Ph/CH₂OH**

Porphyrin **Ph/CH₂OH** was crystallized from THF upon slow vapor diffusion of heptane. The dominant organization in the crystal displays coordination polymers with adjacent porphyrins in a staircase arrangement (Fig. 4a). Each zinc atom is pentacoordinate. The hydroxymethyl group of one porphyrin is coordinated to the apical site of the zinc atom of the adjacent porphyrin (O–Zn distance 2.1564(18) Å (Fig. S11a)), while the angle C–O–Zn is 136.94(15)° (Fig. S11a). Although the apical coordination of the hydroxymethyl group is clearly displayed, the remaining hydroxyl group is orientationally disordered. When a given hydroxyl group is pointed toward the zinc atom, the nearest hydroxyl group from the adjacent double staircase hydrogen-bonds with the hydroxyl group coordinated to zinc. The O(hydroxymethyl oxygen)–H distance when participating in the O–H···O hydrogen bond along the tract is 1.87(4) Å (Fig. 4b), which is well within the range of known hydrogen bonds.³⁶ Thus, hydrogen bonding may exist between hydroxyl groups in adjacent staircases.

A given coordination polymer of apical-ligated porphyrins is aligned alongside a second polymer of apical-ligated porphyrins. The angle between the two staircases is 72.66(3)° (Fig. 4b). The *meso*-phenyl groups are neither coplanar nor orthogonal with respect to the plane of the porphyrin, as is typical; here, both phenyl groups are tilted in the same direction with dihedral angles of 115.15(7)° and 108.82(7)° (Fig. S11a). The plane of the phenyl group on the porphyrin from the second staircase is rotated 75.37(10)° versus that from the first one, affording a putative CH/π interaction (2.687(3) Å) between two phenyl groups from adjacent

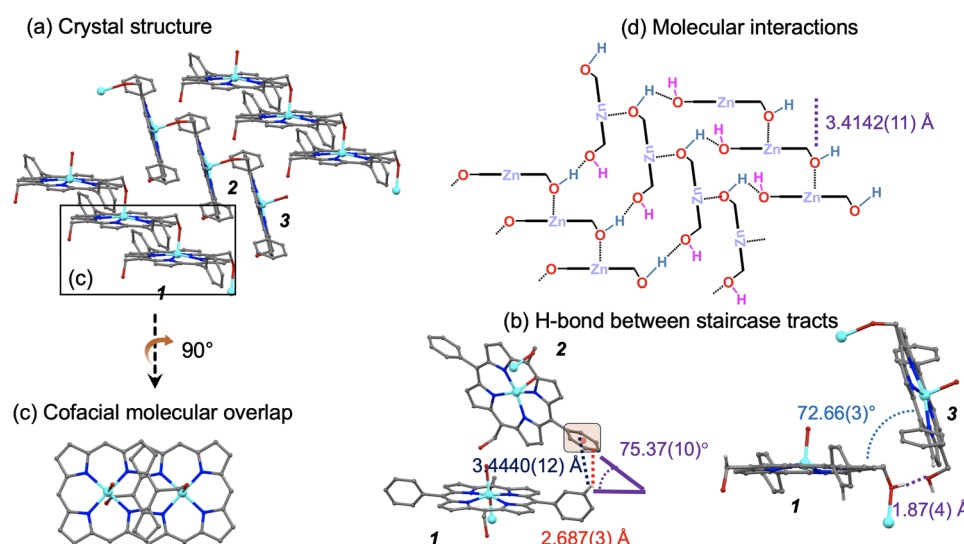


Fig. 4 Zinc porphyrin **Ph/CH₂OH** (pentacoordinate zinc atoms). (a) Packing arrangement showing a section of infinite coordination polymer of porphyrins. The hydroxymethyl of one porphyrin ligates to the apical zinc site of a second porphyrin. Two adjacent polymers form a double staircase containing inner tract hydroxymethyl moieties in the crystal structure. (b) Possible hydrogen-bonding between staircase tracts. The labels **1–3** correspond to porphyrins shown in panel (a). (c) Top view showing the partial cofacial overlap between two adjacent porphyrins in a staircase. Many substituents are omitted for clarity. (d) Illustration of proposed molecular interactions in the assembly of **Ph/CH₂OH**.



staircases, along with the distance to the centroid belonging to the mentioned phenyl group at 3.4440(12) Å (Fig. 4b).

Although the planes of porphyrins in adjacent staircases are not parallel, the planes of every other staircase are parallel giving an overall herringbone arrangement. The two adjacent macrocycles are slipped from a completely cofacial alignment to give only partial overlap of the π clouds (Fig. 4c). The distance along the normal between the mean planes of two porphyrins in a coordination polymer is 3.4142(11) Å (Fig. 4d). The resulting translation is such that the centroid offset of porphyrins in adjacent steps is 5.3177(11) Å (Fig. S11a). The two infinite polymers thus constitute a side-by-side or double staircase comprised of cofacially offset porphyrins, which altogether affords a zigzag shape. A model for the assembly showing the key interactions of the central zinc metal and two hydroxymethyl groups is provided in Fig. 4d.

Porphyrin H/CH₂OH

Porphyrin H/CH₂OH was crystallized from THF upon slow vapor diffusion of acetonitrile. The dominant organization in the crystal involves coordination polymers. Each zinc atom is hexacoordinate. Each hydroxymethyl group on one porphyrin coordinates at the apical site of the zinc atom on an adjacent porphyrin (Fig. 5a). Thus, each porphyrin donates two apically coordinating hydroxymethyl groups and receives two apically coordinating hydroxymethyl groups. The four nearest porphyrin neighbors to a given porphyrin display essentially orthogonal planes thereto (90.28(3)°) (Fig. 5b). The angle C–O–Zn is 115.85(10)°, while the O–Zn distance is 2.3504(14) Å (Fig. S11b).

The two hydroxymethyl groups of a given porphyrin are oriented in a *trans*-configuration with respect to each other. The O–H bonds are not uncompensated due to the presence of molecules of acetonitrile in the crystal lattice (two CH₃CN per porphyrin; in other words, one CH₃CN for each hydroxymethyl group). Each hydroxymethyl group serves as a hydrogen-bond donor with the nitrogen atom of a molecule of acetonitrile (Fig. 5c). The H···N distances are 2.14(3) Å. The acetonitrile molecules are aligned in pairs with dipoles in opposite directions, with a distance of 3.983(4) Å from the methyl carbon of

one acetonitrile molecule to the nitrogen atom of the other acetonitrile molecule (Fig. 5b). The oppositely aligned dimers of acetonitrile are solvent molecules in the porphyrin lattice.

The four adjacent, apically coordinated porphyrins form a square-shaped arrangement around a central porphyrin. Although such nearest neighbors have essentially orthogonal planes, the next-nearest neighbor porphyrins are coplanar with each other but are translated such that there is essentially no cofacial overlap. A model for the assembly showing the key interactions of the central zinc metal, two hydroxymethyl groups, and the presence of the acetonitrile molecules, is provided in Fig. 5c.

Porphyrin Ph/Et

Porphyrin Ph/Et was crystallized from THF upon slow vapor diffusion of hexane. Each zinc is hexacoordinate, which is derived from two molecules of THF (Fig. 6a). The O(THF)–Zn distance is 2.4495(12) Å, and each THF oxygen is ligated to the zinc at an angle nearly normal 78.81(6)° *versus* the mean plane (Fig. S11c). Further, the zinc metal works as an inversion center of the molecule. Both phenyl groups are tilted in the same direction (dihedral angle of 70.59(5)°), whereas the ethyl groups are pointed in opposite directions relative to the plane of the macrocycle (Fig. S11c). The distance between two mean planes is 3.3400(15) Å (Fig. 6c), whereas the closest contact (2.3902(3) Å) in the same plane is observed between the *para*-positions of phenyl C–H atoms (Fig. 6b). The two adjacent macrocycles are slipped with no discernible interplanar overlap (Fig. 6c).

Porphyrin H/Et

Porphyrin H/Et was crystallized from THF upon slow vapor diffusion of acetone. The packing pattern shows a zigzag pattern of adjacent staircases of porphyrins (Fig. 7a). While the appearance may resemble that of 1, here there is no opportunity for heteroatom ligation to the zinc centers (from one porphyrin to another), and indeed, each zinc atom is tetracoordinate. The angle between the two staircases is 79.05(4)° (Fig. 7a). A putative CH/π interaction (2.7993(15) Å) from H7 to the macrocycle between adjacent staircases, along with the distance to the centroid belonging to the mentioned macrocycle at 4.9470(8) Å are shown in Fig. 7b. The two adjacent macrocycles are slipped

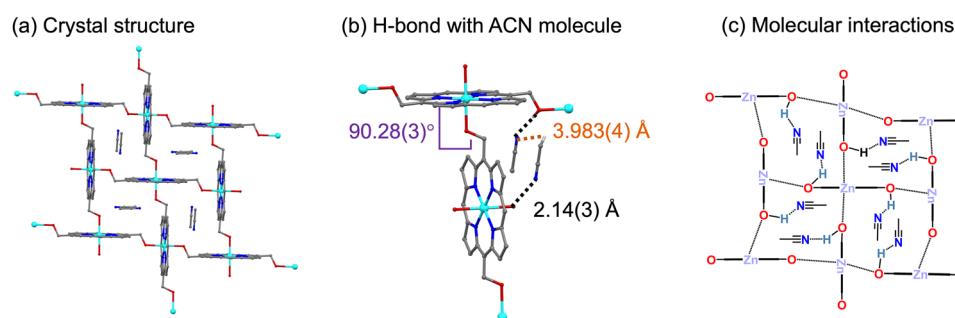


Fig. 5 Zinc porphyrin H/CH₂OH (hexacoordinate zinc atoms). (a) Packing arrangement showing a section of the infinite coordination polymer of porphyrins. (b) Hydrogen bond between an acetonitrile molecule and a hydroxymethyl group (black dotted lines) and distances between acetonitrile molecules (orange dotted lines). (c) Illustration of proposed molecular interactions in the assembly of H/CH₂OH. Many substituents are omitted for clarity.



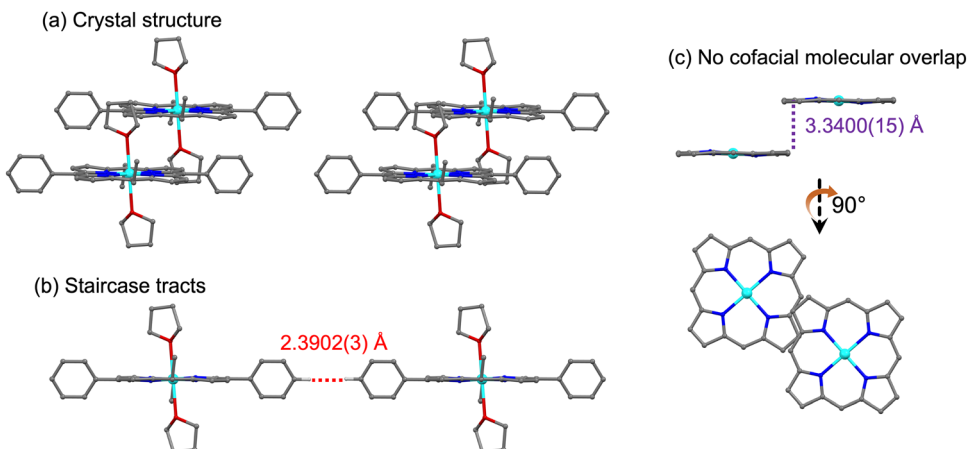


Fig. 6 Zinc porphyrin **Ph/Et** (hexacoordinate zinc atoms). (a) Packing arrangement showing a section of infinite coordination polymer of porphyrins. (b) Staircase tract of **Ph/Et**. (c) Top view showing no cofacial overlap.

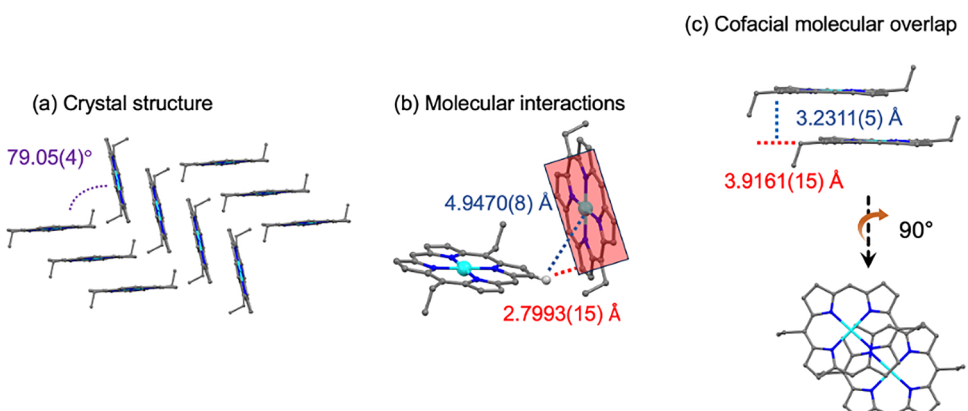


Fig. 7 Zinc porphyrin **H/Et** (tetracoordinate zinc atoms). (a) Packing arrangement. (b) Staircase tract of **H/Et**. (c) Top view showing the partial cofacial overlap between two adjacent porphyrins in a staircase.

from a completely cofacial alignment to give only partial overlap of the π clouds. The resulting translation is such that the centroid offset of porphyrins in adjacent steps is 3.9161(15) Å (Fig. 7c). The distance between the two mean planes is 3.2311(5) Å (Fig. 7c).

Outlook

Efforts to understand the structural organization underpinning aggregates of native chlorin macrocycles, such as those found in green photosynthetic bacteria, have prompted studies of model tetrapyrrole systems. The first question of interest concerns the essential structural features that engender self-assembly. The second question concerns how much structural deviation – in the nature of the substituted tetrapyrrole macrocycle – can be present yet still achieve efficient light harvesting, *i.e.*, absorption of light and delivery of an exciton to a designated site. Almost all work to date, including that herein, focuses on the first question.

Here, zinc porphyrins are employed rather than magnesium chlorins (as in the native systems, *e.g.*, BChl *c*). Both porphyrins

Ph/CH₂OH and **H/CH₂OH** contain 5,15-bis(hydroxymethyl) substituents but contain or lack 10,20-diphenyl substituents. Both afford infinite coordination polymers by ligation of a hydroxymethyl group at the apical zinc site. But otherwise the crystal packing patterns are fundamentally different. In **Ph/CH₂OH**, where phenyl groups are present, each zinc is pentacoordinate and a double staircase results in which adjacent porphyrins within a staircase are aligned along the 5,15-axis, with separation of mean planes of the two porphyrins of 3.4142(11) Å and a cofacial offset of 5.3177(11) Å; the adjacent staircases are linked by hydrogen-bonding. In **H/CH₂OH**, where phenyl groups are absent, each zinc is hexacoordinate, the four nearest neighbors coordinated to a given porphyrin display orthogonal planes in a square-like architecture, and two molecules of acetonitrile per porphyrin in the crystal lattice serve as hydrogen-bond acceptors of the O–H derived from apical coordination; there is no cofacial π -overlap of adjacent porphyrins. Whether incorporation of acetonitrile (or another moiety) is essential for this pattern of solid-state assembly remains to be determined. More broadly, a next step concerns the all-important second question – the extent to which these, or any other crystalline-like assemblies – can

support the remarkable light-harvesting features found in native systems.

Experimental section

General methods

All ^1H NMR spectra (500 MHz, 600 MHz, 700 MHz) and $^{13}\text{C}\{^1\text{H}\}$ NMR spectra (125 MHz, 150 MHz, 175 MHz) were recorded at room temperature. Mass spectra of porphyrins were obtained by MALDI-MS using the matrix α -cyano-4-hydroxycinnamic acid (CHCA) or 1,4-bis(5-phenyloxazol-2-yl)benzene (POPOP).²⁸ Absorption spectra were collected in toluene or THF at room temperature. Silica gel (40 μm average particle size) and alumina (80–200 mesh) were used for column chromatography. All reagents were used as received. Dry THF was distilled over Na/benzophenone. CHCl_3 contained ethanol as an inhibitor.

Noncommercial samples

Dipyrromethane **1**,²² dipyrromethane **6**,²⁶ and *S*-2-pyridyl benzothioate **7**²⁷ were obtained as described in the literature.

Synthesis procedures

Dibutyl[5,10-dihydro-1,9-dibenzoyl-5-(*tert*-butyldimethylsilyloxy)methyl]dipyrinatotin(IV) (2)²². Following a literature procedure²² at 3-fold larger scale than reported, mesitylmagnesium bromide (1.0 M in THF, 10 mL, 10 mmol) was added dropwise to a solution of **1** (2.15 g, 7.41 mmol) in distilled toluene (15 mL) in an ice bath. The reaction mixture was stirred at 0 °C for 30 min. Benzoyl chloride (1.85 mL, 15.8 mmol) was added dropwise, and the resulting mixture was stirred at 0 °C for 1 h. The reaction mixture was poured into a mixture of saturated aqueous NH_4Cl solution and ethyl acetate. The organic layer was separated, washed with brine, dried (Na_2SO_4), and concentrated. The resulting yellow oil was dissolved in ethyl acetate (60 mL) at room temperature and treated with triethylamine (3.1 mL) and Bu_2SnCl_2 (2.25 g, 7.41 mmol) for 30 min. The reaction mixture was washed with water and brine, dried (Na_2SO_4), and concentrated. Chromatography [silica, hexanes/ CH_2Cl_2 (1:2 with 0.5% triethylamine)] yielded a yellow viscous oil (2.92 g, 54%). ^1H NMR (CDCl_3 , 500 MHz) δ –0.14 (s, 6H), 0.61 (t, J = 7.3 Hz, 3H), 0.84 (s, 2H), 0.96–1.03 (m, 2H), 1.12–1.18 (m, 2H), 1.31–1.36 (m, 4H), 1.56–1.62 (m, 4H), 1.77–1.81 (m, 2H), 3.78 (d, J = 7.3 Hz, 2H), 4.46 (t, J = 7.3 Hz, 1H), 6.44 (d, J = 3.7 Hz, 2H), 7.11 (d, J = 3.7 Hz, 2H), 7.49–7.58 (m, 6H), 7.90–7.91 (m, 4H); $^{13}\text{C}\{^1\text{H}\}$ NMR (CDCl_3 , 125 MHz) δ –5.7, 13.7, 13.8, 18.6, 23.2, 25.5, 25.9, 26.1, 26.8, 27.2, 27.8, 43.7, 71.3, 116.1, 123.9, 128.5, 129.2, 131.7, 136.3, 137.9, 150.0, 184.6. HRMS (ESI-TOF) m/z : [M + H]⁺ calcd for $\text{C}_{38}\text{H}_{51}\text{N}_2\text{O}_3\text{SiSn}$ 731.2691; found 731.2700.

5,15-Di(*tert*-butyldimethylsilyloxy)methyl-10,20-diphenylporphyrin (3)²². Following a literature procedure,²² a sample of NaBH_4 (522 mg, 13.8 mmol) was added in portions to a stirred solution of **2** (503 mg, 0.690 mmol) in THF/methanol (10:1, 40 mL). The progress of the reaction was followed by TLC. The reaction was complete in 40 min, at which point the reaction mixture was quenched by the addition of water and then poured

into CH_2Cl_2 . The organic phase was separated, washed with water, dried (Na_2SO_4), and concentrated to give the dipyrromethane-1,9-dicarbinol as a yellow oil. The latter was immediately subjected to condensation with dipyrromethane **1** (200 mg, 0.690 mmol) in the presence of InCl_3 (19.1 mg, 0.0863 mmol) in CH_2Cl_2 (80 mL) for 90 min. Then, DDQ (680 mg, 3 mmol) was added to the reaction mixture. The reaction mixture was stirred for 20 min. Then, triethylamine (5 mL) was added. The crude mixture was concentrated to dryness and then purified by chromatography [silica, hexanes/ CH_2Cl_2 (1:1)] to obtain a purple solid (26 mg, 5%). The title compound could not be dissolved in CH_2Cl_2 , CHCl_3 , DMSO or THF but was analyzed by mass spectrometry and absorption spectroscopy. MALDI-MS (CHCA) obsd 750.31, calcd 750.38 ($\text{C}_{46}\text{H}_{54}\text{N}_4\text{O}_2\text{Si}_2$); λ_{abs} (toluene) 416, 514, 544, 592 nm.

Zinc(II) 5,15-di(*tert*-butyldimethylsilyloxy)methyl-10,20-diphenylporphyrin (4). Following a general procedure⁴ with some modification, a solution of **3** (17.2 mg, 0.0230 mmol) in CHCl_3 (7 mL) was treated with a suspension of $\text{Zn}(\text{OAc})_2$ (252 mg, 1.15 mmol) in methanol (1.75 mL). The resulting mixture was stirred overnight at room temperature. The mixture was washed with water and extracted with CH_2Cl_2 . The organic extract was dried (Na_2SO_4) and then concentrated under reduced pressure. Chromatography [silica, hexanes/ CH_2Cl_2 (1:3 with 0.5% triethylamine)] yielded a purple solid (12.8 mg, 68%). ^1H NMR (CDCl_3 , 600 MHz) δ 0.22 (s, 12H), 0.98 (s, 18H), 7.04 (s, 4H), 7.77–7.80 (m, 6H), 8.22 (d, J = 7.2 Hz, 4H), 9.03 (d, J = 3.0 Hz, 4H), 9.68 (d, J = 3.6 Hz, 4H). $^{13}\text{C}\{^1\text{H}\}$ NMR (CDCl_3 , 175 MHz) δ –4.5, 26.2, 29.9, 64.9, 117.0, 120.7, 126.7, 127.6, 129.5, 132.6, 134.6, 143.0, 150.1, 150.8. The title compound was not highly soluble in CDCl_3 . MALDI-MS (CHCA) obsd 812.08, calcd 812.29 ($\text{C}_{46}\text{H}_{52}\text{N}_4\text{O}_2\text{Si}_2\text{Zn}$); λ_{abs} (toluene + two drops of THF) 422, 554, 586 nm.

Zinc(II) 5,15-di(*tert*-butyldimethylsilyloxy)methyl-10,20-diphenylporphyrin (5). Following a literature procedure²⁵ with modification, a solution of **3** (145 mg, 0.500 mmol) in CH_2Cl_2 (5 mL) at room temperature was treated with *N,N*-dimethylmethyleneammonium iodide (Eschenmoser's reagent; 194 mg, 1.05 mmol). After 1 h, CH_2Cl_2 (4 mL) and saturated aqueous NaHCO_3 (3 mL) were added to the reaction mixture. The organic phase was dried (Na_2SO_4) and then concentrated to dryness to afford crude **1-Esch**. A solution of crude **1-Esch** and dipyrromethane **1** (145 mg, 0.500 mmol) in ethanol (50 mL) at room temperature was treated with $\text{Zn}(\text{OAc})_2$ (1.10 g, 5.00 mmol). The mixture was heated to reflux. After 2 h, the reaction mixture was allowed to cool to room temperature. A sample of DDQ (340 mg, 1.50 mmol) was added, and the mixture was stirred for 30 min. Triethylamine (355 μL , 2.50 mmol) was added, and the reaction mixture was concentrated to dryness. Column chromatography [silica, hexanes/ CH_2Cl_2 1:1 with 0.5% triethylamine] afforded a purple solid (38 mg, 11.5%). ^1H NMR (DMSO-d_6 , 500 MHz) δ 0.25 (s, 12H), 0.93 (s, 18H), 7.12 (s, 4H), 9.57 (d, J = 4.5 Hz, 4H), 9.82 (d, J = 4.0 Hz, 4H), 10.29 (s, 2H); $^{13}\text{C}\{^1\text{H}\}$ NMR (DMSO-d_6 , 175 MHz) δ –4.7, 18.1, 25.9, 64.3, 105.5, 115.1, 129.8, 132.2, 148.7, 149.9; MALDI-MS (CHCA) obsd 660.19, calcd 660.23 ($\text{C}_{34}\text{H}_{44}\text{N}_4\text{O}_2\text{Si}_2\text{Zn}$). HRMS (ESI-TOF) m/z : [M + HCOO][–] calcd for $\text{C}_{35}\text{H}_{45}\text{N}_4\text{Si}_2\text{O}_6$ 705.2276; found 705.2287; λ_{abs} (toluene + two drops of THF) 412, 544, 580 nm.



1-Benzoyl-5-ethylidipyrromethane (8). Following a literature procedure²⁶ with modification, a solution of dipyrromethane 6 (308 mg, 1.77 mmol) in THF (1.77 mL) was treated with EtMgBr (4.5 mL, 4.5 mmol, 1.0 M in THF) under argon. The mixture was stirred at room temperature for 10 min and then cooled to -78°C . A solution of *S*-2-pyridyl benzothioate (7, 381 mg, 1.77 mmol) in THF (1.77 mL) was then added dropwise. The solution was maintained at -78°C for 20 min. Analysis by TLC [silica; dichloromethane/ethyl acetate (100 : 3)] showed complete consumption of the pyridyl thioester after 20 min, so the cooling bath was removed. The reaction mixture was poured into a mixture of saturated aqueous NH₄Cl solution and ethyl acetate. The organic layer was separated, washed with brine, dried (Na₂SO₄), and concentrated to afford a yellow oil. Purification by flash column chromatography [silica; neat CH₂Cl₂ to CH₂Cl₂/ethyl acetate (100 : 3)] afforded a yellow oil (441 mg, 90%). ¹H NMR (CDCl₃, 500 MHz) δ 0.95 (t, *J* = 7.5 Hz, 3H), 2.09–2.15 (m, 2H), 4.03 (t, *J* = 8.0 Hz, 1H), 6.05–6.07 (m, 1H), 6.10 (dd, *J* = 3.5 Hz, 6.0 Hz, 1H), 6.18 (dd, *J* = 2.5 Hz, 3.5 Hz, 1H), 6.83 (dd, *J* = 2.5 Hz, 4.0 Hz, 1H), 7.47 (t, *J* = 8.0 Hz, 2H), 7.56 (t, *J* = 7.5 Hz, 1H), 7.84–7.85 (m, 2H), 8.91 (brs, 1H), 10.47 (brs, 1H); ¹³C{¹H} NMR (CDCl₃, 125 MHz) δ 12.6, 27.3, 40.2, 105.5, 108.2, 109.3, 117.4, 122.3, 128.5, 129.0, 130.4, 131.9, 132.2, 138.7, 144.5, 185.1; HRMS (ESI-TOF) *m/z*: [M + Na]⁺ calcd for C₁₈H₁₈N₂ONa 301.1317; found 301.1312.

5,15-Diethyl-10,20-diphenylporphyrin (9). Following a literature procedure²⁶ with modification, a sample of NaBH₄ (473 mg, 12.5 mmol) was carefully added in small portions to a stirred solution of dipyrromethane 8 (139 mg, 0.5 mmol) in THF/methanol (3 : 1, 10 mL). Analysis by TLC [silica; hexanes/ethyl acetate (9 : 1)] showed complete consumption of 8 after 20 min, so the reaction mixture was quenched by the addition of water and CH₂Cl₂. The organic layer was separated, washed with brine, dried (Na₂SO₄), and concentrated to afford the dipyrromethane-1-carbinol as a yellow oil. The crude dipyrromethane-1-carbinol was immediately dissolved in acetonitrile (100 mL), and TFA (231 μ L, 3 mmol, 30 mM) was added. After 10 min, DDQ (227 mg, 1 mmol) was added, and the mixture was stirred at room temperature for 1 h. Then, triethylamine (417 μ L, 3 mmol) was added. The crude mixture was concentrated to dryness and then purified by chromatography [alumina, hexanes/CH₂Cl₂ (1 : 1)] to afford a purple solid (48 mg, 37%). ¹H NMR (CDCl₃, 700 MHz) δ –2.69 (s, 2H), 2.13 (t, *J* = 7.7 Hz, 6H), 5.02 (q, *J* = 7.7 Hz, 4H), 7.75–7.81 (m, 6H), 8.20 (d, *J* = 7.0 Hz, 4H), 8.87 (d, *J* = 4.2 Hz, 4H), 9.45 (d, *J* = 4.2 Hz, 4H); ¹³C{¹H} NMR (CDCl₃, 175 MHz) δ 22.9, 28.8, 119.0, 121.3, 126.7, 127.7, 134.6, 134.7, 142.8, resonances from the α - and β -carbons of the porphyrin were not observed; MALDI-MS (CHCA) obsd 518.24, calcd 518.25 (C₃₆H₃₀N₄); λ_{abs} (toluene) 419, 516, 549, 653 nm.

Zinc(ii) 5,15-bis(hydroxymethyl)-10,20-diphenylporphyrin (Ph/CH₂OH). Following a literature procedure²² with modification, a solution of 4 (12.8 mg, 0.0157 mmol) in THF (1.7 mL) under argon was treated with TBAF (1.0 M in THF, 236 μ L, 0.24 mmol) at room temperature for 9 h. The mixture was washed with water and extracted with CH₂Cl₂. The organic extract was concentrated. The crude product as a solid was added to the top of a small Celite

pipette and washed with CH₂Cl₂ to remove impurities. The resulting solid on top of the pipette was then treated with distilled THF to achieve solubilization of the porphyrin and subsequent elution. The filtrate was concentrated to dryness to yield a purple solid (7.0 mg, 76%). ¹H NMR (DMSO-*d*₆, 500 MHz) δ 6.02 (t, *J* = 6.0 Hz, 2H), 6.70 (d, *J* = 5.5 Hz, 4H), 7.69–7.70 (m, 6H), 8.04 (dd, *J* = 6.9 Hz, 2.1 Hz, 4H), 8.69 (d, *J* = 4.6 Hz, 4H), 9.62 (d, *J* = 4.7 Hz, 4H); ¹³C{¹H} NMR (DMSO-*d*₆, 175 MHz) δ 62.7, 118.0, 119.5, 126.7, 127.5, 130.0, 131.5, 134.3, 143.0, 149.0, 150.2; MALDI-MS (POPOP) obsd 584.27, calcd 584.12 (C₃₄H₂₄N₄O₂Zn); λ_{abs} (toluene + two drops of THF) 423, 555 nm. A single crystal from THF/heptane was examined by SCXRD analysis.

Zinc(ii) 5,15-bis(hydroxymethyl)porphyrin (H/CH₂OH). Following a literature procedure²² with modification, a solution of 5 (23.2 mg, 0.035 mmol) in THF (3.8 mL) under argon was treated with TBAF (1.0 M in THF, 525 μ L, 0.53 mmol) at room temperature for 9 h. The mixture was washed with water and extracted with CH₂Cl₂. The organic extract was concentrated. The crude product was washed with CH₂Cl₂ through a small Celite pipette to remove impurities. The resulting solid on top of the pipette was then treated with distilled THF to achieve solubilization of the porphyrin and subsequent elution. The filtrate was concentrated to dryness to yield a purple solid (13.6 mg, 90%). ¹H NMR (DMSO-*d*₆, 500 MHz) δ 6.13 (t, *J* = 6.0 Hz, 2H), 6.91 (d, *J* = 5.5 Hz, 4H), 9.54 (d, *J* = 4.5 Hz, 4H), 9.88 (d, *J* = 4.5 Hz, 4H), 10.27 (s, 2H); ¹³C{¹H} NMR (DMSO-*d*₆, 175 MHz) δ 62.5, 105.2, 116.7, 130.1, 131.9, 148.6, 150.1; MALDI-MS (CHCA) obsd 432.05, calcd 432.06 (C₂₂H₁₆N₄O₂Zn); HRMS (ESI-TOF) *m/z*: [M + HCOO][–] calcd for C₂₃H₁₇N₄O₄Zn 477.0547; found 477.0552; λ_{abs} (toluene + two drops of THF) 410, 543, 578 nm. A single crystal obtained from THF/CH₃CN was examined by SCXRD analysis.

Zinc(ii) 5,15-diethylporphyrin (H/Et). Following a literature procedure²⁵ with modification, a solution of 6 (131 mg, 0.750 mmol) in CH₂Cl₂ (7.5 mL) at room temperature was treated with *N,N*-dimethylmethylenammonium iodide (Eschenmoser's reagent; 291 mg, 1.58 mmol). After 1 h, CH₂Cl₂ (6 mL) and saturated aqueous NaHCO₃ (4.5 mL) were added to the reaction mixture. The organic phase was dried (Na₂SO₄) and then concentrated to dryness to afford crude 6-Esch. A solution of crude 6-Esch and dipyrromethane 6 (131 mg, 0.750 mmol) in ethanol (75 mL) at room temperature was treated with Zn(OAc)₂ (1.65 g, 7.50 mmol). The mixture was heated to reflux. After 2 h, the reaction mixture was allowed to cool to room temperature. A sample of DDQ (510 mg, 2.25 mmol) was added, and the mixture was stirred for 15 min. Triethylamine (532 μ L, 3.75 mmol) was added, and the reaction mixture was concentrated to dryness. Column chromatography [silica, hexanes/CH₂Cl₂ (3 : 1) with 0.5% triethylamine] gave a solid. The solid was washed several times with hexanes/CH₂Cl₂ (5 : 1) to remove impurities, affording a purple solid (27 mg, 8.3%). ¹H NMR (THF-*d*₈, 700 MHz) δ 2.16 (t, *J* = 7.7 Hz, 6H), 5.19 (q, *J* = 7.7 Hz, 4H), 9.40 (d, *J* = 4.2 Hz, 4H), 9.71 (d, *J* = 4.9 Hz, 4H), 10.08 (s, 2H); ¹³C{¹H} NMR (THF-*d*₈, 175 MHz) δ 23.8, 29.5, 105.4, 121.2, 129.6, 132.6, 149.9, 150.9; MALDI-MS (CHCA) obsd 428.10, calcd 428.10 (C₂₄H₂₀N₄Zn); HRMS (ESI-TOF) *m/z*: [M]⁺ calcd for



$C_{24}H_{20}N_4Zn$ 428.0979; found 428.0978; λ_{abs} (toluene + two drops of THF) 413, 546 nm. A single crystal obtained from THF/acetone was examined by SCXRD analysis.

Zinc(II) 5,15-diethyl-10,20-diphenylporphyrin (Ph/Et). Following a general procedure⁴ with some modification, a solution of **9** (11.2 mg, 21.6 μ mol) in $CHCl_3$ (8 mL) was treated with a suspension of $Zn(OAc)_2$ (231 mg, 1.05 mmol) in methanol (2 mL). The resulting mixture was stirred overnight at room temperature. The mixture was washed with water and extracted with CH_2Cl_2 . The organic extract was dried (Na_2SO_4) and then concentrated under reduced pressure. The resulting solid was washed several times with hexanes/ CH_2Cl_2 (5 : 1) to remove impurities, affording a purple solid (10 mg, 80%). 1H NMR ($THF-d_8$, 700 MHz) δ 2.11 (t, J = 7.7 Hz, 6H), 5.12 (q, J = 7.7 Hz, 4H), 7.73–7.78 (m, 6H), 8.18 (d, J = 7.0 Hz, 4H), 8.85 (d, J = 4.2 Hz, 4H), 9.56 (d, J = 4.2 Hz, 4H); $^{13}C\{^1H\}$ NMR ($THF-d_8$, 175 MHz) δ 23.7, 29.7, 120.3, 122.5, 127.2, 128.1, 129.1, 132.7, 135.5, 145.1, 150.4, 151.0; MALDI-MS (CHCA) obsd 580.21, calcd 580.16 ($C_{36}H_{28}N_4Zn$); HRMS (ESI-TOF) m/z : [M]⁺ calcd for $C_{36}H_{28}N_4Zn$ 580.1605; found 580.1608; λ_{abs} (toluene + two drops of THF) 426, 557 nm. A single crystal obtained from THF/hexane was examined by SCXRD analysis.

Measurement of steady-state absorption and emission

Each porphyrin was examined in a THF solution in air at room temperature. Absorption spectra were measured with a Shimadzu UV-2600i spectrophotometer using a spectral bandwidth of 1.0 nm and a medium scan rate (500 nm/3 min). Emission measurements were collected using a Horiba Canada-Fluorolog-QM™ using a bandpass of 5 nm, 1-nm step sizes, and an integration time of 1 s. The samples were excited at the wavelength of the respective B bands: porphyrin **Ph/CH₂OH** at 421 nm, **H/CH₂OH** at 408 nm, **H/Et** at 410 nm, and **Ph/Et** at 424 nm.

Time-resolved spectroscopy measurements

(i) Sample preparation of **Ph/CH₂OH** and **H/CH₂OH**. Porphyrins **Ph/CH₂OH** and **H/CH₂OH** were dissolved in tetrahydrofuran (THF) followed by sonication for 5 min to ensure a uniform concentration.

(ii) Fluorescence lifetime measurements from time-correlated single photon counting (TCSPC). Fluorescence lifetimes were measured for 20 μ M solutions of **Ph/CH₂OH** and **H/CH₂OH** in a 10-mm excitation and 2-mm emission pathlength cuvette. A 20 μ M solution of **ZnTPP** was also prepared in THF solution for comparison. All the porphyrin solutions were excited at 550 nm using a 10-nm band pass filter. To generate the excitation pulse, an 800 nm centered femtosecond 80 MHz pulse, produced by a mode-locked Ti:sapphire pulsed laser (Mai Tai HP, Spectra Physics) was first focused into a nonlinear photonic crystal fiber (FemtoWhite800, NKT Photonics) to generate a white light supercontinuum. This beam was passed through a 10-nm band pass filter at 550 nm, selected for the excitation wavelength of 550 nm. The emission from the sample was isolated using another 10-nm bandpass filter (**ZnTPP** and **Ph/CH₂OH** at 650 nm; **H/CH₂OH** at 635 nm). Single photons from the fluorescence emission were then detected by a single-photon avalanche diode (Micro Photon

Devices) connected to a time-correlated single photon module (PicoHarp 300, Picoquant) to record the arrival times, producing a histogram of photon events up to \sim 12 ns.

The impulse response function (IRF) was similarly measured with a colloidal silica (LUDOX) solution sample. The fluorescence lifetimes were then calculated by performing a deconvolution of the IRF with an exponential fit optimized by a least-squares regression.

(iii) Ultrafast transient absorption (TA) measurements. Solutions of **Ph/CH₂OH** and **H/CH₂OH** (100 μ M in THF) were used for femtosecond TA measurements. Both samples were measured using a 2-mm flow-cuvette set up to control photodegradation. Both porphyrins were measured with pump powers of 20 nJ per pulse with time delays from \sim 25 ps to 1.3 ns. The experimental apparatus has been described.^{37,38} In brief, the femtosecond transient absorption measurements were taken with a femtosecond 400 nm pump pulse and a broadband white light supercontinuum probe. The instrument response function measured through the pump–probe cross-correlation from a frequency-resolved optical gating (FROG) experiment was \sim 250 fs. Both pulses were sourced from the 800 nm mode-locked output of a Ti:Sapphire laser (Coherent Libra) with a repetition rate of 5 kHz. Splitting this output in two, one path was sent through an argon tube pressurized at 20 psi to generate the broadband white light continuum used as the probe. The second beam path was used to generate the pump pulse at 400 nm through second harmonic generation after passing through a BBO crystal. The pump was chopped using a 2.5 kHz optical chopper to create a repetition rate half that of the probe to obtain the delta absorbance (ΔA) signal. The time delay between the pump and probe pulses was set by a motorized delay stage (Aerotech) which controlled the path length of the pump. For the transient absorption measurements, both pulses were then focused and spatially overlapped onto the sample. The transmitted probe was then dispersed using a holographic grating (450 grooves per mm, Wasatch Photonics) and detected by a 2048-pixel CCD camera (e2v Aviiva EM4). All data analysis was done using home-built code in MATLAB-R2023a.

Density functional theory calculations

DFT calculations were performed with Gaussian 16 version C.01.³³ The calculations used the PCM model in toluene. The optimized molecular geometries, energies, and electron density distributions were obtained using the long-ranged corrected ω B97XD functional and the 6-31++G** basis set.

SCXRD analyses

For each of the four compounds, the diffraction data were collected at 100 K using a Bruker D8 Venture diffractometer ($MoK\alpha$, 0.71073 \AA) equipped with APEX³⁹ software. The crystal structure was calculated, integrated, and processed using SAINT,⁴⁰ SHELXL,⁴¹ and OLEX2⁴² software. All calculations for crystallographic distances and angles were analyzed by OLEX2 software. The crystallographic information file (CIF) for porphyrins **H/CH₂OH** (2496240), **Ph/Et** (2496241), **H/Et** (2496247), and **Ph/CH₂OH** (2496248) can be retrieved at <https://www.ccdc.cam.ac.uk>.



Conflicts of interest

The authors declare no competing financial interest.

Data availability

Supplementary information (SI): assignments of the ^1H NMR spectra for selected porphyrins; absorption and fluorescence spectra; time-resolved fluorescence data; calculation of radiative and nonradiative decay rates; Gouterman 4-orbital calculations and simulated spectra; SCXRD data for four porphyrins; ^1H and $^{13}\text{C}\{^1\text{H}\}$ NMR spectra for new compounds. See DOI: <https://doi.org/10.1039/d5nj04118j>.

CCDC 2496240 (**H/CH₂OH**), 2496241 (**Ph/Et**), 2496247 (**H/Et**), and 2496248 (**Ph/CH₂OH**) contain the supplementary crystallographic data for this paper.^{43a-d}

All other data are contained in the paper.

Acknowledgements

This work was supported by grants from the Division of Chemical Sciences, Geosciences, and Biosciences, Office of Basic Energy Sciences of the U.S. Department of Energy (DE-SC0025243 to G. S. S.-C., DE-SC0025317 to J. S. L.). G. S. S.-C. acknowledges a Camille-Dreyfus Teacher-Scholar Award for support. M. N. S. acknowledges support from the NSF Graduate Research Fellowship Program and from a MathWorks Science Fellowship. Compound characterization was performed by the Molecular Education, Technology and Research Innovation Center (METRIC) at NC State University, which is supported by the State of North Carolina. SCXRD data were obtained at University of Tennessee at Knoxville.

References

- 1 B. R. Green, J. M. Anderson and W. W. Parson, in *Light-Harvesting Antennas in Photosynthesis*, ed. B. R. Green and W. W. Parson, *Advances in Photosynthesis and Respiration*, Kluwer Academic Publishers, The Netherlands, 2003, vol. 13, pp. 1–28.
- 2 R. E. Blankenship, J. M. Olson and M. Miller, in *Anoxygenic photosynthetic bacteria*, ed. R. E. Blankenship, M. T. Madigan and C. E. Bauer, *Advances in Photosynthesis*, Kluwer Academic Publishers, The Netherlands, 1995, pp. 399–435.
- 3 H. Scheer, in *Chlorophylls and Bacteriochlorophylls: Biochemistry, Biophysics, Functions and Applications*, ed. B. Grimm, R. J. Porra, W. Rüdiger and H. Scheer, *Advances in Photosynthesis and Respiration*, Springer, The Netherlands, 2006, pp. 1–26.
- 4 M. Ptaszek, Z. Yao, D. Savithri, P. D. Boyle and J. S. Lindsey, *Tetrahedron*, 2007, **63**, 12629–12638.
- 5 H. Tamiaki, M. Kouraba, K. Takeda, S.-I. Kondo and R. Tanikaga, *Tetrahedron:Asymmetry*, 1998, **9**, 2101–2111.
- 6 T. Miyatake, H. Tamiaki, A. R. Holzwarth and K. Schaffner, *Helv. Chim. Acta*, 1999, **82**, 797–810.
- 7 V. I. Prokhortenko, A. R. Holzwarth, M. G. Müller, K. Schaffner, T. Miyatake and H. Tamiaki, *J. Phys. Chem. B*, 2002, **106**, 5761–5768.
- 8 Y. Saga, S. Akai, T. Miyatake and H. Tamiaki, *Chem. Lett.*, 2004, **33**, 544–545.
- 9 T. S. Balaban, H. Tamiaki and A. R. Holzwarth, *Top. Curr. Chem.*, 2005, **258**, 1–38.
- 10 S. Sasaki and H. Tamiaki, *J. Org. Chem.*, 2006, **71**, 2648–2654.
- 11 H. Tamiaki, K. Hamada and M. Kunieda, *Tetrahedron*, 2008, **64**, 5721–5727.
- 12 T. Miyatake and H. Tamiaki, *Coord. Chem. Rev.*, 2010, **254**, 2593–2602.
- 13 T. S. Balaban, A. Eichhöfer and J.-M. Lehn, *Eur. J. Org. Chem.*, 2000, 4047–4057.
- 14 T. S. Balaban, A. D. Bhise, M. Fischer, M. Linke-Schaetzel, C. Roussel and N. Vanthuyne, *Angew. Chem., Int. Ed.*, 2003, **42**, 2140–2144.
- 15 T. S. Balaban, M. Linke-Schaetzel, A. D. Bhise, N. Vanthuyne and C. Roussel, *Eur. J. Org. Chem.*, 2004, 3919–3930.
- 16 T. S. Balaban, M. Linke-Schaetzel, A. D. Bhise, N. Vanthuyne, C. Roussel, C. E. Anson, G. Buth, A. Eichhöfer, K. Foster, G. Garab, H. Gliemann, R. Goddard, T. Javorfi, A. K. Powell, H. Rösner and T. Schimmel, *Chem. – Eur. J.*, 2005, **11**, 2267–2275.
- 17 T. S. Balaban, *Acc. Chem. Res.*, 2005, **38**, 612–623.
- 18 M. C. Balaban, A. Eichhöfer, G. Buth, R. Hauschild, J. Szmytkowski, H. Kalt and T. S. Balaban, *J. Phys. Chem. B*, 2008, **112**, 5512–5521.
- 19 T. Jochum, C. M. Reddy, A. Eichhöfer, G. Buth, J. Szmytkowski, H. Kalt, D. Moss and T. S. Balaban, *Proc. Natl. Acad. Sci. U. S. A.*, 2008, **105**, 12736–12741.
- 20 T. S. Balaban, A. D. Bhise, G. Bringmann, J. Bürck, C. Chappaz-Gillot, A. Eichhöfer, D. Fenske, D. C. G. Götz, M. Knauer, T. Mizoguchi, D. Mössinger, H. Rösner, C. Roussel, M. Schraut, H. Tamiaki and N. Vanthuyne, *J. Am. Chem. Soc.*, 2009, **131**, 14480–14492.
- 21 T. S. Balaban, in *Handbook of Porphyrin Science*, ed. K. M. Kadish, K. M. Smith and R. Guillard, World Scientific Publishing Co., Singapore, 2010, ch. 3, vol. 1, pp. 221–306.
- 22 Z. Yao, J. Bhaumik, S. Dhanalekshmi, M. Ptaszek, P. A. Rodriguez and J. S. Lindsey, *Tetrahedron*, 2007, **63**, 10657–10670.
- 23 L. De Cola and W. Schuhmann, *ChemPlusChem*, 2017, **82**, 511–512.
- 24 C. M. Carcel, J. K. Laha, R. S. Loewe, P. Thamyonkit, K.-H. Schweikart, V. Misra, D. F. Bocian and J. S. Lindsey, *J. Org. Chem.*, 2004, **69**, 6739–6750.
- 25 D. Fan, M. Taniguchi, Z. Yao, S. Dhanalekshmi and J. S. Lindsey, *Tetrahedron*, 2005, **61**, 10291–10302.
- 26 P. D. Rao, B. J. Littler, G. R. Geier III and J. S. Lindsey, *J. Org. Chem.*, 2000, **65**, 1084–1092.
- 27 D. K. Dogutan, M. Ptaszek and J. S. Lindsey, *J. Org. Chem.*, 2008, **73**, 6187–6201.
- 28 N. Srinivasan, C. A. Haney, J. S. Lindsey, W. Zhang and B. T. Chait, *J. Porphyrins Phthalocyanines*, 1999, **3**, 283–291.
- 29 N. C. M. Magdaong, M. Taniguchi, J. R. Diers, D. M. Niedzwiedzki, C. Kirmaier, J. S. Lindsey, D. F. Bocian and D. Holten, *J. Phys. Chem. A*, 2020, **124**, 7776–7794.
- 30 M. Taniguchi, J. S. Lindsey, D. F. Bocian and D. Holten, *J. Photochem. Photobiol. C*, 2021, **46**, 100401.
- 31 S. Akimoto, T. Yamazaki, I. Yamazaki and A. Osuka, *Chem. Phys. Lett.*, 1999, **309**, 177–182.



32 B. Abraham, J. Nieto-Pescador and L. Gundlach, *J. Phys. Chem. Lett.*, 2016, **7**, 3151–3156.

33 M. J. Frisch, G. W. Trucks, H. B. Schlegel, G. E. Scuseria, M. A. Robb, J. R. Cheeseman, G. Scalmani, V. Barone, G. A. Petersson, H. Nakatsuji, X. Li, M. Caricato, A. V. Marenich, J. Bloino, B. G. Janesko, R. Gomperts, B. Mennucci, H. P. Hratchian, J. V. Ortiz, A. F. Izmaylov, J. L. Sonnenberg, D. Williams-Young, F. Ding, F. Lipparini, F. Egidi, J. Goings, B. Peng, A. Petrone, T. Henderson, D. Ranasinghe, V. G. Zakrzewski, J. Gao, N. Rega, G. Zheng, W. Liang, M. Hada, M. Ehara, K. Toyota, R. Fukuda, J. Hasegawa, M. Ishida, T. Nakajima, Y. Honda, O. Kitao, H. Nakai, T. Vreven, K. Throssell, J. A. Montgomery, Jr., J. E. Peralta, F. Ogliaro, M. J. Bearpark, J. J. Heyd, E. N. Brothers, K. N. Kudin, V. N. Staroverov, T. A. Keith, R. Kobayashi, J. Normand, K. Raghavachari, A. P. Rendell, J. C. Burant, S. S. Iyengar, J. Tomasi, M. Cossi, J. M. Millam, M. Klene, C. Adamo, R. Cammi, J. W. Ochterski, R. L. Martin, K. Morokuma, O. Farkas, J. B. Foresman and D. J. Fox, Gaussian, Inc., Wallingford CT, 2019.

34 A. K. Mandal, M. Taniguchi, J. R. Diers, D. M. Niedzwiedzki, C. Kirmaier, J. S. Lindsey, D. F. Bocian and D. Holten, *J. Phys. Chem. A*, 2016, **120**, 9719–9731.

35 H. Du, M. Taniguchi, J. R. Diers, C. Kirmaier, D. F. Bocian, J. S. Lindsey and D. Holten, *Photochem. Photobiol.*, 2025, **101**, 869–885.

36 G. A. Jeffrey, *An introduction to hydrogen bonding*, Oxford University Press, New York, 1997.

37 J. I. Ogren, A. L. Tong, S. C. Gordon, A. Chenu, Y. Lu, R. E. Blankenship, J. Cao and G. S. Schlau-Cohen, *Chem. Sci.*, 2018, **9**, 3095–3104.

38 D. Wang, O. C. Fiebig, D. Harris, H. Toporik, Y. Ji, C. Chuang, M. Nairat, A. L. Tong, J. I. Ogren, S. M. Hart, J. Cao, J. N. Sturgis, Y. Mazor and G. S. Schlau-Cohen, *Proc. Natl. Acad. Sci. U. S. A.*, 2023, **120**, e2220477120.

39 Bruker, *Bruker APEX5*, Bruker AXS Inc., Madison, Wisconsin, USA, 2023.

40 Bruker, *Bruker SAINT*, Bruker AXS Inc., Madison, Wisconsin, USA, 2023.

41 G. M. Sheldrick, *Acta Crystallogr., Sect. C: Struct. Chem.*, 2015, **71**, 3–8.

42 O. V. Dolomanov, L. J. Bourhis, R. J. Gildea, J. A. K. Howard and H. Puschmann, *J. Appl. Crystallogr.*, 2009, **42**, 339–341.

43 (a) CCDC 2496240: Experimental Crystal Structure Determination, 2025, DOI: [10.5517/ccdc.csd.cc2psjwx](https://doi.org/10.5517/ccdc.csd.cc2psjwx); (b) CCDC 2496241: Experimental Crystal Structure Determination, 2025, DOI: [10.5517/ccdc.csd.cc2psjxy](https://doi.org/10.5517/ccdc.csd.cc2psjxy); (c) CCDC 2496247: Experimental Crystal Structure Determination, 2025, DOI: [10.5517/ccdc.csd.cc2psj35](https://doi.org/10.5517/ccdc.csd.cc2psj35); (d) CCDC 2496248: Experimental Crystal Structure Determination, 2025, DOI: [10.5517/ccdc.csd.cc2psk46](https://doi.org/10.5517/ccdc.csd.cc2psk46).

